

# Lightweight Learning from Actuation-Space Demonstrations via Flow Matching for Whole-Body Soft Robotic Grasping

Liudi Yang<sup>†</sup>, Yang Bai<sup>†</sup>, Yuhao Wang<sup>†</sup>, Ibrahim Alsarraj, Gitta Kutyniok, Zhanchi Wang\*, Ke Wu\*

**Abstract**—Robotic grasping under uncertainty remains a fundamental challenge due to its uncertain and contact-rich nature. Traditional rigid robotic hands, with limited degrees of freedom and compliance, rely on complex model-based and heavy feedback controllers to manage such interactions. Soft robots, by contrast, exhibit embodied mechanical intelligence: their underactuated structures and passive flexibility of their whole body, naturally accommodate uncertain contacts and enable adaptive behaviors. To harness this capability, we propose a lightweight actuation-space learning framework that infers distributional control representations for whole-body soft robotic grasping, directly from deterministic demonstrations using a flow matching model (Rectified Flow), without requiring dense sensing or heavy control loops. Using only 30 demonstrations (less than 8% of the reachable workspace), the learned policy achieves a 97.5% grasp success rate across the whole workspace, generalizes to grasped-object size variations of  $\pm 33\%$ , and maintains stable performance when the robot’s dynamic response is directly adjusted by scaling the execution time from 20% to 200%. These results demonstrate that actuation-space learning, by leveraging its passive redundant DOFs and flexibility, converts the body’s mechanics into functional control intelligence and substantially reduces the burden on central controllers for this uncertain-rich task.

**Index terms**— Soft Robotics; Whole-body Grasping; Actuation-Space Learning from Demonstrations; Rectified Flow; Distributional Control; Embodied Mechanical Intelligence

## I. INTRODUCTION

Robotic grasping under uncertainty remains a central challenge due to its uncertain and contact-rich nature [1]. These tasks involve high-dimensional, nonlinear, and uncertain dynamics, making them inherently difficult to model and control [2]. Traditional rigid robotic hands, with limited degrees of freedom and low compliance, often exhibit poor adaptability and safety when interacting under such conditions. Soft robots, by contrast, embody mechanical intelligence [3]: their intrinsic redundancy, flexibility, and compliance of their whole body, allow them to passively absorb uncertainty, enabling safe and adaptive physical interaction while reducing reliance on precise centralized control [4]. Despite these morphological advantages, developing motion planning and control strategies for soft robots remains challenging [5]. Their dynamics are high-dimensional and history-dependent, while uncertain contacts resulting from friction [6], material fatigue [7], and geometric constraints [8] further complicate both planning and real-time control.

Existing approaches on the control of soft robots can be broadly categorized into model-based [5] and learning-based methods [9]. Model-based control relies on explicit

physical formulations, ranging from piecewise constant curvature (PCC) models [10] and pseudo-rigid-body approximations [8], to geometrically nonlinear beam and rod theories [11], [12], and finite-element or solid-mechanics-based approaches [13], [14]. These controllers offer interpretable descriptions of soft-body mechanics and can often guarantee stability or convergence. However, their practical deployment is hindered by high modeling complexity [11], [12], computationally expensive inverse solutions [13], and large sim-to-real discrepancies arising from material and contact uncertainties [15], [16]. Consequently, purely model-based control remains difficult to scale and lacks robustness when dealing with unmodeled deformations or uncertain interactions.

In contrast, learning-based control circumvents explicit modeling by leveraging data [9]. Artificial neural networks (ANNs) have been widely adopted in soft robotics for tasks such as kinematics, dynamics, and state estimation [17]. For instance, ANNs have been used to approximate the inverse statics of cable-driven soft arms [18], to model forward dynamics for predictive control [19], and to implement imitation learning policies for soft robotic hands trained from human demonstrations [20]. With their universal function approximation capability [21], ANNs can capture nonlinear dynamics directly from data without explicit physical models. However, their accuracy and generalization strongly depend on the amount and quality of training data, and limited demonstrations often constrain their robustness and adaptability [22]. While this suffices for low-level tasks [9], these methods generally fail to cope with *robotic manipulation scenarios* involving strong dynamics and significant uncertainty [23]. To move beyond supervised imitation, reinforcement learning (RL) has been explored as an alternative that enables autonomous exploration and policy optimization [24]. In soft robotics, RL has been demonstrated in locomotion and basic trajectory tracking, such as soft snake robots [25] and continuum arms [19], [26], yet applications to whole-body grasping remain scarce [17]. Although RL can theoretically surpass expert demonstrations, it is notoriously sample inefficient, requires carefully engineered rewards, and poses safety risks on hardware [7], [24]. More recently, Diffusion Policy (DP) has achieved impressive performance in rigid robot visuomotor control, modeling multimodal action distributions and handling high-dimensional spaces [27]. Extensions include on-device diffusion transformers [28], hierarchical policies for multi-task manipulation [29], and 3D visual representations [30]. Despite their success, diffusion-based methods require multi-step denoising at inference, introducing latency and significant computational cost [27].

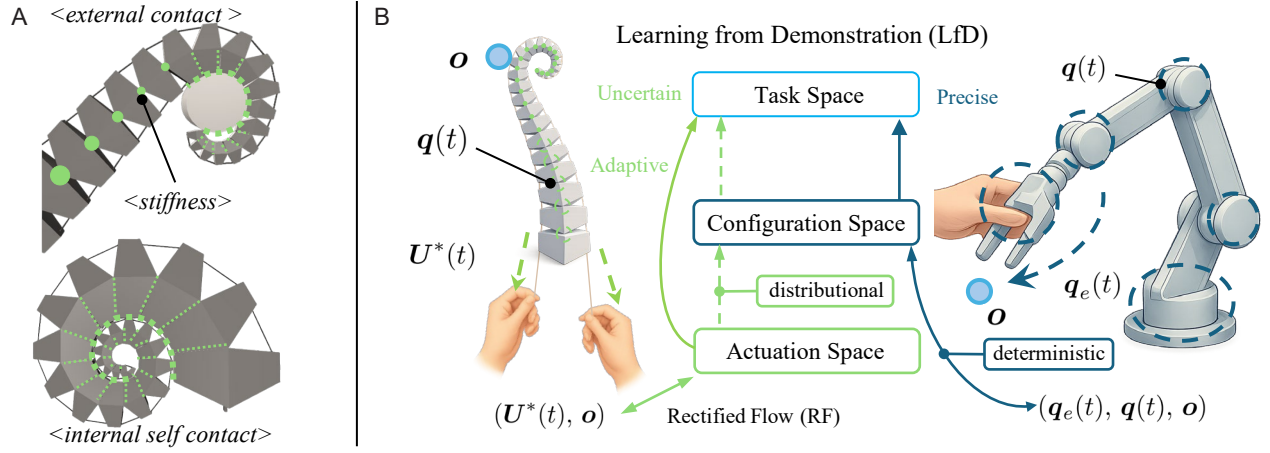


Fig. 1. Learning from Actuation-Space Demonstration for Grasping. A. SpiRob. B. Distinction in LfD schemes between rigid and soft robots.

Such precise and high-frequency closed-loop corrections may not align with the nature of soft robots, which inherently exhibit nonlinearities, uncertain contacts, and history dependence [3], [6]. In soft robotic systems, embodied mechanical intelligence, arising from redundancy, flexibility, and compliance, already absorbs part of the uncertainty [3], [4], suggesting that increasingly heavy computation may not yield proportional benefits.

These observations motivate a lightweight distributional control framework that generates robust patterns, preserves multimodality, and leverages the embodied mechanical intelligence of soft robots to handle uncertainty. A natural solution is Learning from Demonstrations (LfD), since expert demonstrations inherently encode feasible and multimodal strategies without requiring explicit modeling or reward design [31]. Performing such learning in actuation space may better exploit the robot’s passive flexibility and redundancy, providing a potential pathway for embodied intelligence to emerge through coordinated actuation behaviors. Building on this idea, we propose a lightweight framework for Learning from actuation-space demonstrations that learns control distributions directly aligned with the soft robot’s physical characteristics. Within this framework, we employ the Rectified Flow (RF) model [32], a flow-matching generative approach that efficiently learns control distributions with minimal sampling [33]. We validate the proposed approach on a spiral-shaped soft robot (SpiRob) [8], performing whole-body grasping under uncertainty. The policy, trained with only 30 demonstrations covering less than 8% of the reachable workspace, achieved a 97.5% grasp success rate across the workspace. It also generalized to objects with size variations of  $\pm 33\%$  and maintained stable grasping performance when the execution duration was scaled between 20% and 200%, demonstrating robust adaptability under uncertainty. The contributions are summarized as follows:

- **Framework.** A lightweight framework for **Learning from actuation-space demonstrations** that couples the **embodied mechanical intelligence** of soft robots with

distributional learning to handle uncertainty.

- **Method.** A concrete implementation using the **Rectified Flow** model, enabling efficient distributional control through flow matching with minimal sampling.
- **Evidence.** Comprehensive validation on a SpiRob showing **strong generalization and robustness** under uncertainty.
- **Insight.** A broader perspective that couples **embodied mechanical intelligence** with **distributional control policies**, **alleviating centralized computation** and enabling reliable whole-body grasping under uncertainty.

## II. PROBLEM STATEMENT

### A. Investigated Soft Robot – SpiRob

Spiral robots (SpiRobs) represent a class of bio-inspired continuum manipulators that take advantage of the geometric regularity of logarithmic spirals [8]. Unlike conventional soft arms with uniform structures, SpiRobs exhibit a natural gradient in stiffness and curvature from base to tip, as shown in Fig. 1A. This intrinsic property enables a wide operational workspace and facilitates smooth transitions between different motion primitives such as reaching, wrapping, and grasping. Their structure can be rapidly prototyped through 3D printing of flexible filaments, such as TPU, while actuation is achieved through a minimal number of tendons. This design reduces mechanical complexity and highlights the fundamental challenge of coordinating many coupled degrees of freedom under complex nonlinear body dynamics. These characteristics make SpiRobs an ideal testbed for exploring data-driven approaches in the context of high-dimensional motion generation and control.

### B. Task Objectives

The task suite focuses on object manipulation within a horizontal workspace, designed to exploit the whole-body compliance of SpiRobs. The primary objective is a planar wrapping grasp, where the robot approaches an object and secures it by sequentially uncurling and curling its spiral body.

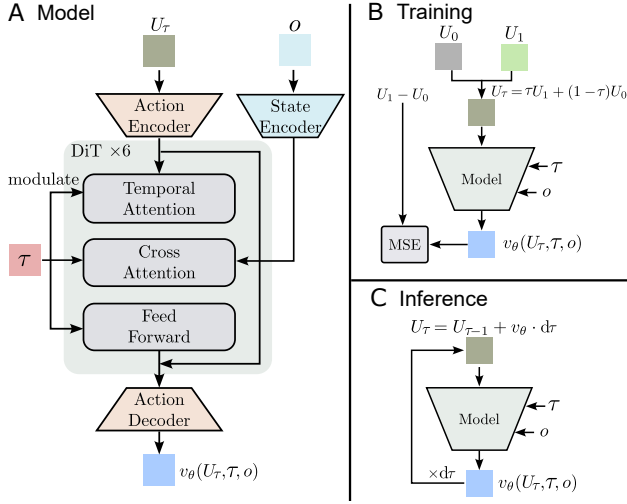


Fig. 2. Illustration of the proposed framework. A. Overview of the model architecture designed to learn the flow. B. Training scheme used for optimization. C. Inference scheme applied at test time.

### III. METHODOLOGY

#### A. Preliminary

1) *Rectified Flow:* Rectified Flow (RF) [32], [33] is a generative flow-matching framework that learns a continuous flow field to transform noise into data, offering a fast and stable alternative to diffusion-based training [34]. The overall training and inference pipeline of the RF model is illustrated in Fig. 2. Originally proposed in computer vision, RF has demonstrated a strong ability to capture complex and multi-modal distributions, enabling more robust and generalizable control than conventional imitation or reinforcement learning [35]. Let  $U_1 \sim \Pi_{\text{data}}$  denote an expert training sample, and  $U_0 \sim \mathcal{N}(0, \mathbb{I})$  a Gaussian noise sample. RF learns a vector field  $v_\tau(U_\tau)$  that continuously transports  $U_0$  to  $U_1$  over the normalized flow time  $\tau \in [0, 1]$ , governed by the ordinary differential equation:

$$\frac{dU_\tau}{d\tau} = v_\tau(U_\tau), \quad \tau \in [0, 1] \quad (1)$$

A simple and natural target for this flow is the straight-line interpolation between  $U_0$  and  $U_1$ :

$$\frac{dU_\tau}{d\tau} = U_1 - U_0 \quad (2)$$

Here,  $(U_1 - U_0)$  represents the target action flow, which means the ideal transport direction from noise to data in the action space. RF parameterizes the flow field using a neural network  $v_\theta(U_\tau, \tau, o)$ , where  $\theta$  are learnable parameters and  $o$  denotes task-specific conditions. The model is optimized using the mean squared error (MSE) between the predicted and target action flows:

$$L = \int_0^1 \mathbb{E}_{U_0, U_1} [\| (U_1 - U_0) - v_\theta(U_\tau, \tau, o) \|^2] d\tau \quad (3)$$

where  $\mathbb{E}$  denotes the expectation over sampled pairs  $(U_0, U_1)$ , and  $\| \cdot \|^2$  denotes the squared Euclidean distance, computed as the sum of squared element-wise differences.

After training, the learned flow field  $v_\theta$  is integrated from  $\tau = 0$  to  $\tau = 1$ , starting from a noise sample  $U_0$ , to generate a new expert-like sequence  $U_1$ . Note that the flow time  $\tau$  is a normalized variable for learning the transport process and is independent of the robot's physical execution time.

2) *Function Representation and Discrete Sampling:* Let  $X \in \mathbb{R}^{N \times d}$  denote a discrete trajectory consisting of  $N$  sampled timesteps within the time interval  $[0, T]$ . The interpolation operator  $\mathcal{I}[\cdot]$ , defined through least-squares curve fitting, maps the discrete samples to a continuous vector function  $X^*(t) \in \mathbb{R}^{1 \times d}$ , which is expressed as

$$X^*(t) = \mathcal{I}[X(t)], \quad t \in [0, T] \quad (4)$$

Conversely, the inverse operator  $\mathcal{I}^{-1}[\cdot]$  uniformly samples  $N$  points from the continuous vector function  $X^*(t)$ , giving the discrete representation:

$$X(t) = \mathcal{I}^{-1}[X^*] = [X^*(t_1), X^*(t_2), X^*(t_3) \dots X^*(t_N)]^T \quad (5)$$

#### B. Training–Inference Framework

1) *Learning from Actuation-Space Demonstration: Soft Robot Dynamics.* Soft robots, being underactuated systems, particularly continuum robots, possess a continuous backbone with a large number degrees of freedom but only a limited number of actuators [10]. The studied SpiRob (Fig. 1A) is modeled in MuJoCo using the concept of pseudo-rigid-body model [36], where the continuous structure is discretized into a chain of rigid segments connected by revolute joints. The resulting dynamics are formulated as

$$M(q)\ddot{q} + C(q, \dot{q}) + G(q) + K(q) + D(q, \dot{q}) = H_c^T(q)U^* + H_e^T(q)u_e, \quad (6)$$

where  $q, \dot{q}, \ddot{q} \in \mathbb{R}^n$  denote the generalized displacement, velocity, and acceleration, respectively.  $M(q)$  represents the inertia matrix,  $C(q, \dot{q})$  the Coriolis and centrifugal effects,  $G(q)$  the gravity vector,  $K(q)$  the stiffness term capturing backbone flexibility, and  $D(q, \dot{q})$  the damping term reflecting internal frictional effects. The actuation mapping matrix  $H_c(q) \in \mathbb{R}^{m \times n}$  is generally rectangular with  $m < n$ , indicating underactuation and a non-bijective mapping between actuation and configuration. According to the definition in Section III-A.2,  $U^*$  explicitly denotes the system input as a continuous function in (6). The investigated SpiRob has a configuration dimension of  $n = 24$  with  $m = 2$  active tendons, clearly exhibiting underactuation. Tendon–robot friction contributes to multiple stable postural configurations [6], while external contact and internal self contact, as shown in Fig. 1A, represented by  $H_e^T(q)u_e$ , introduce the strong nonlinear behaviors [8]. Each tendon's geometric displacement is then defined as

$$\Delta l_i = l_i(q) - l_i(q_0), \quad i = 1, 2. \quad (7)$$

where  $l_i(q)$  denotes the tendon length at configuration  $q$ , and  $l_i(q_0)$  its reference length at the undeformed configuration  $q_0 = \mathbf{0}$ .

**Rigid Robot Dynamics.** In contrast, rigid robots are fully actuated systems, where the generalized coordinates  $q(t)$  and the actuation input  $U^*(t)$  are uniquely related through:

$$M(q)\ddot{q} + C(q, \dot{q}) + G(q) + D(q, \dot{q}) = H(q)_c^T U^* + H_e^T(q)u_e \quad (8)$$

TABLE I

Robot	Task Space	Configuration Space	Actuation Space
Rigid	Precise	Deterministic	Deterministic
Soft	Uncertain	Adaptive	Distributional

where  $H(q)_c \in \mathbb{R}^{n \times n}$  is a square full-rank matrix. This bijective mapping between actuation and configuration spaces allows demonstrations to be directly performed in the configuration space. During demonstration, dragging the end-effector along a desired trajectory  $q_e(t)$  uniquely determines the joint configurations  $q(t)$ . The resulting  $q(t)$  is directly converted by the low-level joint displacement controller into the control signal  $U^*(t)$ , ensuring deterministic and repeatable actuation.

**Comparison and Motivation.** Rigid robots, benefiting from full actuation, allow precise configuration-space teaching and deterministic control. They are inherently suited for high-precision and repeatable tasks in well-defined environments but become limited when facing dynamic interactions with high uncertainty, such as grasping, unless equipped with high-frequency, model-based feedback control. In contrast, soft robots are underactuated and possess high degrees of freedom. Their configuration  $q$  cannot be directly controlled due to underactuation, yet this very property, together with passive compliance, allows the actuation space to fully express their embodied mechanical intelligence. Learning in the actuation space therefore exploit and amplify these intrinsic features, enabling adaptive behaviors to emerge through coordinated actuation. Consequently, demonstrations for soft robots are conducted in the actuation space, where each sample is represented as a control–task pair. Therefore, demonstrations for soft robots are instead performed in the actuation space, where each sample is represented as a control–task pair:

$$(U^*(t), o) \quad (9)$$

with  $U^*(t)$  denoting the demonstrated control sequence and  $o$  representing the task condition. Training in this actuation space allows soft robots to directly learn the correspondence between actuation inputs and task outcomes, avoiding the need for explicit and accurate inverse modeling from configuration to actuation and enabling robust adaptation to contact-rich environments (Fig. 1B). A concise comparison of rigid and soft robots in terms of task, configuration, and actuation spaces is summarized in Table I.

2) *Model Architecture:* To learn the control strategy of SpiRobs in whole-body grasping under uncertainty via RF, we develop a MuJoCo-based training framework forming the foundation of our model architecture. As illustrated in Fig. 2A, the proposed rectified-flow model, conditioned on the task condition which is object state  $o \in \mathbb{R}^C$  in this studied case, learns an approximated flow field  $v_\theta(U_\tau, \tau, o)$  that transforms Gaussian noise  $U_0 \in \mathbb{R}^{N \times 2}$  into the expert control sequence  $U_1 \in \mathbb{R}^{N \times 2}$  for the studied SpiRob, where  $C$  denotes the dimension of the object state and  $N$  the number of timesteps. The detailed implementation procedure is summarized in Algorithm 1.

The input action interpolation  $U_\tau = (1 - \tau)U_0 + \tau U_1$

**Algorithm 1** Rectified Flow for Learning Actions of SpiRob

```

1 def train_step(batch):
2     state, target_action = batch
3     cond = state_encoder(state)
4     tau = rand()           # normalized flow time
5     U0 = randn()           # Gaussian noise
6     U1 = target_action      # expert control
7     target_flow = U1 - U0
8     U_tau = U0 + tau * target_flow
9     pred_flow = model(U_tau, tau, cond)
10    loss = mse(pred_flow, target_flow)
11    return loss
12
13 def inference_step(state):
14     cond = state_encoder(state)
15     U = randn()
16     for k in range(k_steps):
17         tau = k / k_steps
18         d_tau = 1 / k_steps
19         pred_flow = model(U, tau, cond)
20         U = U + pred_flow * d_tau
21     return U

```

is processed by the Action Encoder, a stack of linear layers mapping each interpolated action to a latent feature representation. A Diffusion Transformer (DiT) [37] backbone learns the rectified flow vector field, with Temporal Attention capturing temporal dependencies and Cross Attention integrating encoded object-state features for precise spatial conditioning [38]. The State Encoder employs linear projections to transform raw object states into compact latent representations suitable for attention-based fusion.

Each expert demonstration, represented as a continuous control trajectory  $U_1^*(t)$ , is discretized using the sampling operator  $\mathcal{I}^{-1}[\cdot]$  (defined in Sec. III-A.2, Eq. 5), yielding  $U_1 = \mathcal{I}^{-1}[U_1^*(t)] \in \mathbb{R}^{N \times 2}$ , which serves as the target reference during training.

For each normalized flow time  $\tau \in [0, 1]$ , the model generates scale, shift, and gate factors to modulate intermediate feature representations within transformer blocks:

$$h' = \gamma \odot (\alpha \odot h + \beta) \quad (10)$$

where  $\alpha$ ,  $\beta$ , and  $\gamma$  denote the scale, shift, and gate factors, respectively. This modulation mechanism adaptively regulates feature magnitudes and ensures consistent evolution of the internal flow representation along  $\tau$ . An Action Decoder, implemented as a convolutional neural network (CNN), maps the latent features back to the target control sequence space.

During training (Fig. 2B), the interpolated action  $U_\tau = (1 - \tau)U_0 + \tau U_1$  is fed into the model, which is optimized by minimizing the mean squared error (MSE) between the predicted and target action flows ( $U_1 - U_0$ ). During inference (Fig. 2C), the model starts from  $U_0$  and iteratively integrates the learned flow field  $v_\theta(U_\tau, \tau, o)$  using the Euler method to reconstruct the final discrete sequence  $\hat{U}_1$  (where the hat symbol ( $\hat{\cdot}$ ) indicates model-inferred quantities). Finally, the continuous control function for execution is obtained as  $\hat{U}_1^*(t) = \mathcal{I}[\hat{U}_1]$  (using the interpolation operator  $\mathcal{I}[\cdot]$  defined in Sec. III-A.2, Eq. 4) to recover temporal continuity for real-robot deployment.



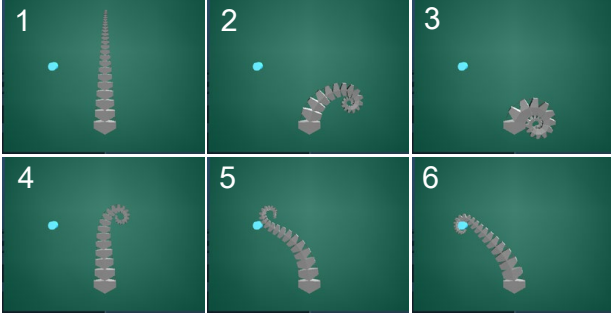


Fig. 3. Example of an expert grasping demo in the simulation.

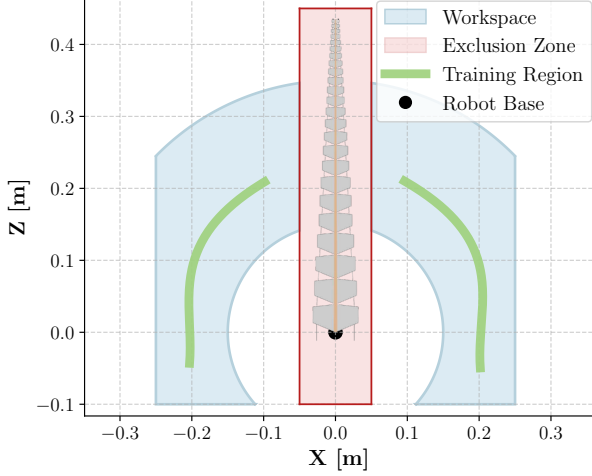


Fig. 4. Workspace and training region configuration for data generation.

#### IV. LEARNING IN SIMULATION

##### A. Simulation and Data Collection

In simulation, the manipulated object moves on a planar surface without rotation, and its state  $o$  is represented by two translational degrees of freedom ( $C = 2$ ). The SpiRob is aligned parallel to the tabletop, ensuring its motion plane coincides with the surface. The object is modeled as a cylinder of 30 mm diameter, placed with its base on the table, as shown in Fig. 3. Physical parameters such as mass, stiffness, and damping follow the settings in [8].

1) *Training Region within the Workspace*: The overall workspace  $\mathcal{R}_{\text{val}}$  is defined as in Fig. 4:

$$\begin{aligned} \mathcal{R}_{\text{val}} = & \left\{ (x, z) \mid r_{\text{in}} \leq \sqrt{(x - x_0)^2 + (z - z_0)^2} \leq r_{\text{out}} \right\} \\ & \cap \left\{ (x, z) \mid x_{\text{min}} \leq x \leq x_{\text{max}} \right\} \cap \left\{ (x, z) \mid z_{\text{min}} \leq z \right\} \\ & \setminus \left\{ (x, z) \mid x_{\text{exc}}^{\text{min}} \leq x \leq x_{\text{exc}}^{\text{max}} \right\} \end{aligned} \quad (11)$$

where  $(x_0, z_0) = (0, 0)$ ,  $r_{\text{in}} = 0.15$  m,  $r_{\text{out}} = 0.35$  m,  $x_{\text{min}} = -0.25$  m,  $x_{\text{max}} = 0.25$  m,  $z_{\text{min}} = -0.1$  m, and the exclusion zone  $x_{\text{exc}}^{\text{min}} = -0.05$  m,  $x_{\text{exc}}^{\text{max}} = 0.05$  m. Within this workspace, a narrow training region (highlighted in green in Fig. 4) was selected for data collection, covering less than 8% of the total workspace area.

2) *Data Collection*: Control is realized in terms of tendon forces that drive the SpiRob's motion. For each expert simulated demo, we record the continuous control function  $U_1^*(t)$ ,

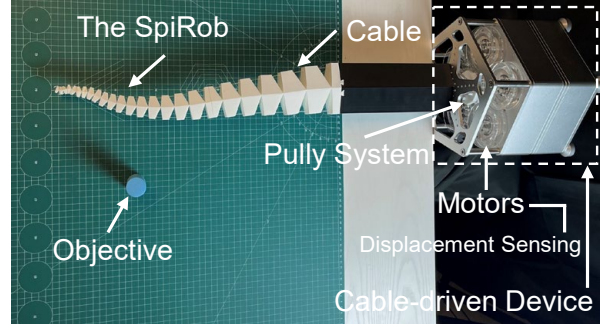


Fig. 5. Experimental setup of the SpiRob platform.

$t \in [0, T]$ , representing the tendon forces over time, together with the corresponding object state  $o \in \mathbb{R}^2$  denoting the sampled placement. The discrete control sequence used for training is then obtained by applying the sampling operator  $\mathcal{I}^{-1}[\cdot]$  to  $U_1$ , yielding  $U_1 = \mathcal{I}^{-1}[U_1^*(t)] \in \mathbb{R}^{N \times 2}$ . Fig. 3 shows a representative expert grasping demo in the simulation, where the robot gradually approaches and encloses the object while  $(U_1, o)$  are recorded for subsequent data processing.

##### B. Training and Inference Details

We collected 30 expert demonstrations in MuJoCo, each providing a continuous expert control function  $U_1^*(t) = [F_1^*, F_2^*]$  with variable duration  $T$  determined by the task completion time, where  $F_1^*$  and  $F_2^*$  denote the left and right tendon control forces. This lightweight learning setup uses a small amount of training data, covering less than 8% of the robot's reachable workspace (Fig. 4). To obtain fixed-length training data, the sampling operator  $\mathcal{I}^{-1}[\cdot]$  was applied to each  $U_1^*(t)$ , yielding a discrete control sequence  $U_1 = [F_1, F_2] = \mathcal{I}^{-1}[U_1^*(t)] \in \mathbb{R}^{N \times 2}$ ,  $N = 80$  represents uniformly sampled timesteps across  $[0, T]$ . The model was trained for 50,000 iterations using the Adam optimizer [39] with a learning rate of  $10^{-4}$  for Eq. 2, on one NVIDIA GeForce RTX 4090 GPU, requiring approximately six hours to complete.

During inference, the rectified flow model was sampled with 30 iteration steps  $\tau$  (Fig. 2C), producing an inferred discrete expert-like control sequence  $\hat{U}_1$ , which is then interpolated using  $\mathcal{I}[\cdot]$  to reconstruct the corresponding continuous expert-like control sequence  $\hat{U}_1^*(t) = [\hat{F}_1^*, \hat{F}_2^*] = \mathcal{I}[\hat{U}_1]$  for execution on the physical robotic platform.

#### V. SIM-TO-REAL EXPERIMENTS

We validate the proposed framework on a SpiRob by transferring the learned policies from simulation to the physical platform. This section first introduces the experimental setup and control-signal processing for sim-to-real transfer, followed by validations in three scenarios: (i) workspace generalization from sparse demonstrations, (ii) geometric adaptability to object size variations, and (iii) robust dynamic scalability.

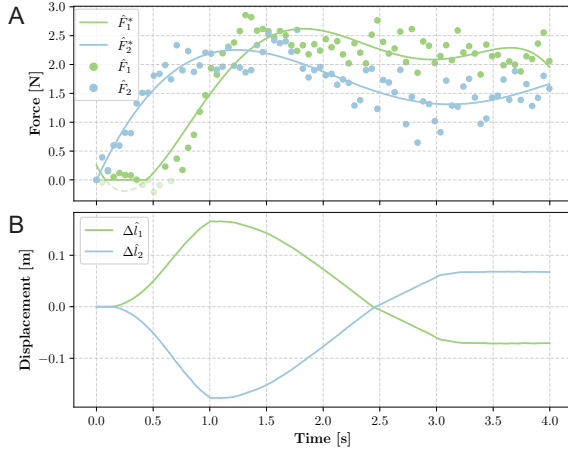


Fig. 6. Control signal interpolation and tendon trajectory generation.

### A. Experimental Setup

1) *Hardware Platform*: The experimental platform is designed to closely mirror the MuJoCo simulation environment (Fig. 5). The physical SpiRob has identical dimensions to the simulated model and is actuated through a cable driven device. This device is powered by high precision joint motors equipped with rotary encoders, allowing accurate control of tendon displacement and thus faithful execution of the commanded trajectories. The robot is mounted on a tabletop with its motion plane aligned parallel to the surface, ensuring consistency with the simulated setup.

2) *Force-to-Displacement Signal Processing for Sim-to-Real Transfer*: Bridging the learned policy from simulation to the physical platform requires a consistent representation of control inputs. In the robot dynamics formulation, tendon actuation appears as control-force terms in the equations of motion (Eq. (6)), directly influencing the dynamic equilibrium of the soft robot. Accordingly, expert demonstrations are represented as continuous control-force functions  $U_1^*(t)$ , and the Rectified Flow model is trained to learn the corresponding force field  $\hat{U}_1^*(t) = [\hat{F}_1^*, \hat{F}_2^*] = \mathcal{I}[\hat{U}_1]$ . As shown in Fig. 6A, the discrete control sequence  $\hat{U}_1 = [\hat{F}_1, \hat{F}_2]$  is interpolated to produce a continuous force function  $\hat{U}_1^*(t)$ , ensuring physical consistency with the underlying dynamics. Here, tendon forces serve as direct control inputs, and the interpolated continuous function  $\hat{U}_1^*(t)$  provides a physically consistent representation for subsequent signal conversion.

On the physical platform, tendon displacement control is adopted because, generally speaking in robotics, displacement control provides a more user-friendly interface than direct force control [40]. For rigid robots, displacement control alone is inadequate for highly dynamic and uncertain interaction tasks, as it cannot explicitly regulate contact forces. In contrast, soft robots inherently exhibit embodied mechanical intelligence, allowing direct control in the actuation space, which enables adaptive and optimized interactions even under displacement control. This approach offers both ease of implementation and the ability to preserve the intrinsic adaptability of soft bodies. Therefore, the hardware executes control through tendon displacement, with motor encoders

providing accurate position feedback. To ensure consistency, the inferred expert-like force trajectories  $\hat{U}_1^*(t)$  are first applied in simulation to compute the corresponding tendon displacement profiles  $\Delta \hat{l}(t)$  (Eq. (7), shown in Fig. 6B), which are then used as executable motor commands.

### B. Experimental Validation

1) *Workspace Generalization from Sparse Demonstrations*: Using the proposed training framework, only 30 demonstrations were collected within a small sampling region, covering less than 8% of the robot's reachable workspace. Despite this limited and localized training data, the learned Rectified Flow policy was evaluated on 1000 uniformly generated target placements across the full workspace, with successful and failed validations shown in different colors in Fig. 7A, achieving a grasping success rate of 97.5%. These results demonstrate that the proposed method enables strong generalization from sparse, small-range training data to diverse unseen positions in the entire workspace, and the grasping behaviors observed in simulation are consistently reproduced on the physical SpiRob platform (Fig. 7B).

2) *Geometric Adaptability to Object Size Variations*: The Rectified Flow policy was trained exclusively on cylindrical objects of 30 mm diameter. During evaluation, the same policy was applied to cylinders of 20 mm (-33%) and 40 mm (+33%) without retraining, and the SpiRob successfully completed the grasping tasks in all cases. These results demonstrate that the learned policy, combined with the robot's embodied mechanical intelligence, enables robust adaptation to object size variations of approximately  $\pm 33\%$ . Representative grasping results are shown in Fig. 7C.

3) *Robust Dynamic Scalability*: The adaptability of the learned policy was further examined under different execution speeds. Starting from a reference displacement trajectory with duration  $T$ , the temporal axis was rescaled to produce faster or slower motions while maintaining the same displacement pattern (Fig. 8). The SpiRob successfully completed grasping with compressed executions up to  $T/5$  and extended executions up to  $2T$ . Within this range, the grasping performance remained stable, indicating that the learned control pattern is robust to temporal scaling and can be directly adjusted by modifying the execution period  $T$ .

## VI. INSIGHTS: DISTRIBUTIONAL CONTROL AND ACTUATION-SPACE DEMONSTRATION

The experimental results in Section V verify the proposed framework on a SpiRob, demonstrating the synergy between embodied mechanical intelligence and a lightweight learning algorithm. These findings reveal key principles underlying distributional control and actuation-space demonstration in soft robotic manipulation.

Soft robots are inherently underactuated, and their configuration  $q$  cannot be uniquely determined from actuator commands. Although this property limits precise configuration-space control, it also provides embodied mechanical intelligence, allowing the robot to passively adapt to contact and

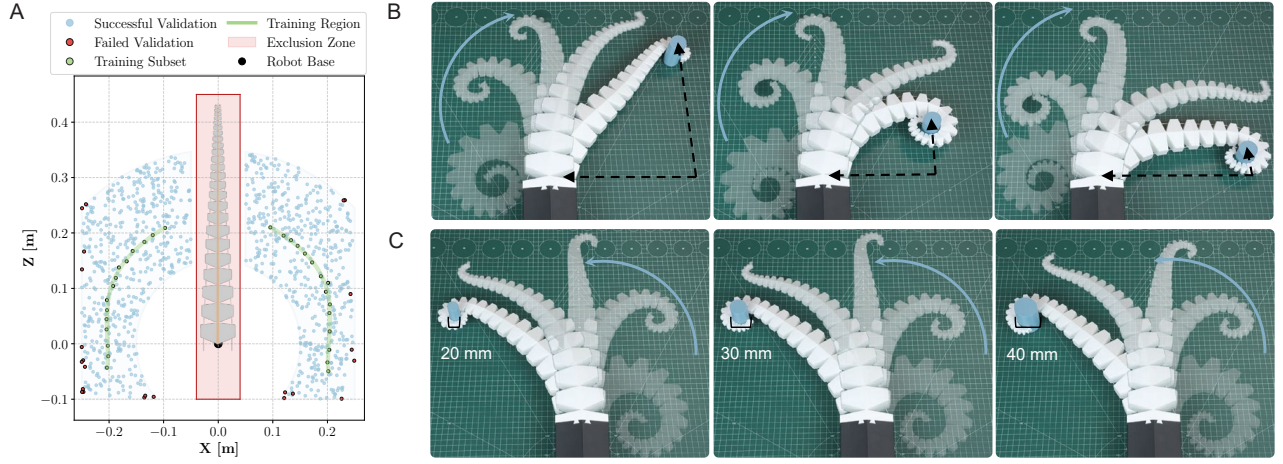


Fig. 7. Experimental results of workspace generalization from sparse demonstrations and geometric adaptability to object size variations

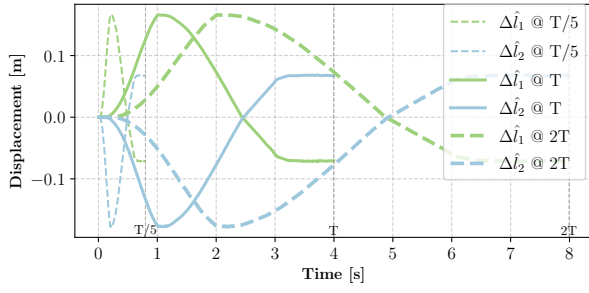


Fig. 8. Experimental results of robust dynamic scalability

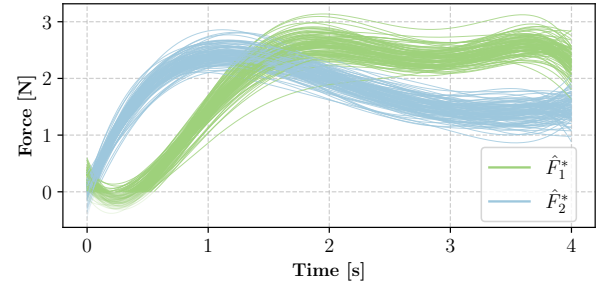


Fig. 9. Distributional sampling of control sequences.

environmental uncertainty through compliance. Such embodiment reduces computational burden and enables the body itself to contribute to control. Demonstrations are therefore more effective in the actuation space, where control inputs correspond directly to tendon forces (Fig. 1B). This representation preserves the physical mapping between actuation and deformation, allowing policies to leverage compliance for adaptive task execution. In contrast, deterministic mappings in configuration space suppress the variability that facilitates adaptation.

Besides, the learned policy exhibits a distributional control pattern. Through the Rectified Flow model, the inferred  $\hat{U}_1$  is inherently discrete and represents the distributional control samples produced by the model, while  $\hat{U}_1^*(t) = [\hat{F}_1^*, \hat{F}_2^*] = \mathcal{I}[\hat{U}_1]$  denotes the corresponding continuous distributional force control functions obtained through least-squares curve fitting respectively. As shown in Fig. 9, 100 sampled force control functions vary individually yet form a consistent distribution, with all executions converging to successful grasps. Rather than encoding a single trajectory, the policy represents a family of feasible control solutions, each providing a different realization through which the robot achieves the same task. This distributional property enhances robustness to uncertainty.

As demonstrated in Fig. 10, the SpiRob performs grasping both in free space (A) and near obstacles (B) using the same actuation-space distribution without explicit replanning or feedback correction. The controller simply provides a

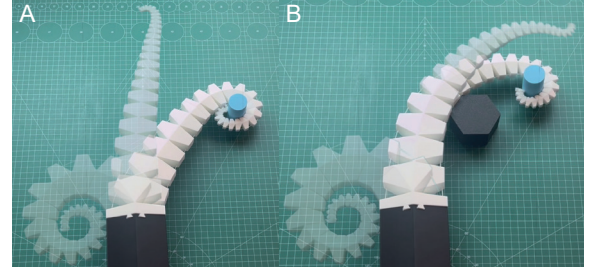


Fig. 10. Whole-body grasping of a SpiRob in uncertain environments.

feasible actuation distribution, while the compliant body autonomously accommodates contact and deformation in real time. This synergy between actuation-space representation and distributional control embodies a broader principle of soft robotic intelligence. It couples embodied mechanical intelligence with distributional control policies, alleviating centralized computation and enabling reliable whole-body grasping under uncertainty.

## VII. CONCLUSIONS

This study presented a lightweight framework for learning from actuation-space demonstrations, which couples embodied mechanical intelligence with distributional control to achieve robust whole-body grasping in soft robots. By employing the Rectified Flow model, the policy efficiently learned coordinated actuation patterns that exploit the inherent compliance and redundancy of the soft body, enabling



adaptive manipulation across diverse conditions. Experiments conducted on a SpiRob demonstrated data-efficient learning from only a small number of demonstrations, strong geometric adaptation to object variations, and scalable dynamic performance under uncertainty. These results confirm that actuation-space learning effectively transforms passive flexibility into functional control intelligence, substantially reducing the reliance on centralized controller. Future work will extend this framework to multi-contact and dynamic manipulation scenarios, and explore hierarchical policy structures for scalable and autonomous soft robotic intelligence.

## REFERENCES

- [1] B. Siciliano, O. Khatib, and T. Kröger, *Springer handbook of robotics*. Springer, 2008, vol. 200.
- [2] M. T. Mason, "Toward robotic manipulation," *Annual Review of Control, Robotics, and Autonomous Systems*, vol. 1, no. 1, pp. 1–28, 2018.
- [3] G. Mengaldo, F. Renda, S. L. Brunton, M. Bächer, M. Calisti, C. Duriez, G. S. Chirikjian, and C. Laschi, "A concise guide to modelling the physics of embodied intelligence in soft robotics," *Nature Reviews Physics*, vol. 4, no. 9, pp. 595–610, 2022.
- [4] R. Pfeifer and J. Bongard, *How the body shapes the way we think: a new view of intelligence*. MIT press, 2006.
- [5] C. Della Santina, C. Duriez, and D. Rus, "Model-based control of soft robots: A survey of the state of the art and open challenges," *IEEE Control Systems Magazine*, vol. 43, no. 3, pp. 30–65, 2023.
- [6] Z. Wang and N. M. Freris, "Exploiting frictional effects to reproduce octopus-like reaching movements with a cable-driven spiral robot," in *2024 IEEE 7th International Conference on Soft Robotics (RoboSoft)*. IEEE, 2024, pp. 537–542.
- [7] T. Chen, Z. Sun, Y. Sun, Y. Wang, D. Song, and K. Wu, "A hybrid hinge-beam continuum robot with passive safety capping for real-time fatigue awareness," *arXiv preprint arXiv:2509.09404*, 2025.
- [8] Z. Wang, N. M. Freris, and X. Wei, "Spirobs: Logarithmic spiral-shaped robots for versatile grasping across scales," *Device*, vol. 3, no. 4, 2025.
- [9] Z. Chen, F. Renda, A. Le Gall, L. Mocellin, M. Bernabei, T. Dangel, G. Ciuti, M. Cianchetti, and C. Stefanini, "Data-driven methods applied to soft robot modeling and control: A review," *IEEE Transactions on Automation Science and Engineering*, vol. 22, pp. 2241–2256, 2024.
- [10] G. S. Chirikjian, "Theory and applications of hyper-redundant robotic manipulators," Ph.D. dissertation, California Institute of Technology, 1992.
- [11] J. Till and D. C. Rucker, "Elastic stability of cosserat rods and parallel continuum robots," *IEEE Transactions on Robotics*, vol. 33, no. 3, pp. 718–733, 2017.
- [12] M. Tummers, V. Lebastard, F. Boyer, J. Troccaz, B. Rosa, and M. T. Chikhaoui, "Cosserat rod modeling of continuum robots from newtonian and lagrangian perspectives," *IEEE Transactions on Robotics*, vol. 39, no. 3, pp. 2360–2378, 2023.
- [13] C. Duriez, "Control of elastic soft robots based on real-time finite element method," in *2013 IEEE international conference on robotics and automation*. IEEE, 2013, pp. 3982–3987.
- [14] B. G. Cangan, S. E. Navarro, B. Yang, Y. Zhang, C. Duriez, and R. K. Katzschmann, "Model-based disturbance estimation for a fiber-reinforced soft manipulator using orientation sensing," in *2022 IEEE/RSJ International Conference on Intelligent Robots and Systems (IROS)*. IEEE, 2022, pp. 9424–9430.
- [15] R. J. Webster III and B. A. Jones, "Design and kinematic modeling of constant curvature continuum robots: A review," *The International Journal of Robotics Research*, vol. 29, no. 13, pp. 1661–1683, 2010.
- [16] G. S. Chirikjian, "Conformational modeling of continuum structures in robotics and structural biology: A review," *Advanced Robotics*, vol. 29, no. 13, pp. 817–829, 2015.
- [17] T. George Thuruthel, Y. Ansari, E. Falotico, and C. Laschi, "Control strategies for soft robotic manipulators: A survey," *Soft robotics*, vol. 5, no. 2, pp. 149–163, 2018.
- [18] M. Girelli, F. Renda, M. Calisti, A. Arienti, G. Ferri, and C. Laschi, "Neural network and jacobian method for solving the inverse statics of a cable-driven soft arm with nonconstant curvature," *IEEE Transactions on Robotics*, vol. 31, no. 4, pp. 823–834, 2015.
- [19] T. G. Thuruthel, E. Falotico, F. Renda, and C. Laschi, "Model-based reinforcement learning for closed-loop dynamic control of soft robotic manipulators," *IEEE Transactions on Robotics*, vol. 35, no. 1, pp. 124–134, 2018.
- [20] A. Gupta, C. Eppner, S. Levine, and P. Abbeel, "Learning dexterous manipulation for a soft robotic hand from human demonstrations," in *2016 IEEE/RSJ International Conference on Intelligent Robots and Systems (IROS)*. IEEE, 2016, pp. 3786–3793.
- [21] Y. LeCun, Y. Bengio, and G. Hinton, "Deep learning," *nature*, vol. 521, no. 7553, pp. 436–444, 2015.
- [22] F. Ebert, Y. Yang, K. Schmeckpeper, B. Bucher, G. Georgakis, K. Daniilidis, C. Finn, and S. Levine, "Bridge data: Boosting generalization of robotic skills with cross-domain datasets," *arXiv preprint arXiv:2109.13396*, 2021.
- [23] T. Osa, J. Pajarinen, G. Neumann, J. A. Bagnell, P. Abbeel, J. Peters *et al.*, "An algorithmic perspective on imitation learning," *Foundations and Trends® in Robotics*, vol. 7, no. 1-2, pp. 1–179, 2018.
- [24] J. Kober, J. A. Bagnell, and J. Peters, "Reinforcement learning in robotics: A survey," *The International Journal of Robotics Research*, vol. 32, no. 11, pp. 1238–1274, 2013.
- [25] X. Liu, C. D. Onal, and J. Fu, "Reinforcement learning of cpg-regulated locomotion controller for a soft snake robot," *IEEE Transactions on Robotics*, vol. 39, no. 5, pp. 3382–3401, 2023.
- [26] S. Satheeshbabu, N. K. Uppalapati, G. Chowdhary, and G. Krishnan, "Open loop position control of soft continuum arm using deep reinforcement learning," in *2019 International Conference on Robotics and Automation (ICRA)*. IEEE, 2019, pp. 5133–5139.
- [27] C. Chi, Z. Xu, S. Feng, E. Cousineau, Y. Du, B. Burchfiel, R. Tedrake, and S. Song, "Diffusion policy: Visuomotor policy learning via action diffusion," *The International Journal of Robotics Research*, vol. 44, no. 10-11, pp. 1684–1704, 2025.
- [28] Y. Wu, H. Wang, Z. Chen, J. Pang, and D. Xu, "On-device diffusion transformer policy for efficient robot manipulation," *arXiv preprint arXiv:2508.00697*, 2025.
- [29] X. Ma, S. Patidar, I. Haughton, and S. James, "Hierarchical diffusion policy for kinematics-aware multi-task robotic manipulation," in *Proceedings of the IEEE/CVF Conference on Computer Vision and Pattern Recognition*, 2024, pp. 18 081–18 090.
- [30] Y. Ze, G. Zhang, K. Zhang, C. Hu, M. Wang, and H. Xu, "3d diffusion policy: Generalizable visuomotor policy learning via simple 3d representations," *arXiv preprint arXiv:2403.03954*, 2024.
- [31] S. Schaal, "Learning from demonstration," *Advances in neural information processing systems*, vol. 9, 1996.
- [32] X. Liu, C. Gong, and Q. Liu, "Flow straight and fast: Learning to generate and transfer data with rectified flow," *arXiv preprint arXiv:2209.03003*, 2022.
- [33] Y. Lipman, R. T. Chen, H. Ben-Hamu, M. Nickel, and M. Le, "Flow matching for generative modeling," *arXiv preprint arXiv:2210.02747*, 2022.
- [34] J. Ho, A. Jain, and P. Abbeel, "Denoising diffusion probabilistic models," *Advances in neural information processing systems*, vol. 33, pp. 6840–6851, 2020.
- [35] Q. Zhang, Z. Liu, H. Fan, G. Liu, B. Zeng, and S. Liu, "Flowpolicy: Enabling fast and robust 3d flow-based policy via consistency flow matching for robot manipulation," in *Proceedings of the AAAI Conference on Artificial Intelligence*, vol. 39, no. 14, 2025, pp. 14 754–14 762.
- [36] L. L. Howell and A. Midha, "A loop-closure theory for the analysis and synthesis of compliant mechanisms," *Journal of Mechanical Design*, vol. 118, no. 1, pp. 121–125, 1996.
- [37] W. Peebles and S. Xie, "Scalable diffusion models with transformers," 2023.
- [38] A. Vaswani, N. Shazeer, N. Parmar, J. Uszkoreit, L. Jones, A. N. Gomez, Ł. Kaiser, and I. Polosukhin, "Attention is all you need," *Advances in neural information processing systems*, vol. 30, 2017.
- [39] D. P. Kingma, "Adam: A method for stochastic optimization," *arXiv preprint arXiv:1412.6980*, 2014.
- [40] J. J. Craig, *Introduction to robotics: mechanics and control*, 3/E. Pearson Education India, 2009.